ADVANCED MATERIALS INTERFACES
Open Access
www.advmatinterfaces.de

Functional Porous Graphene Membranes: From Superhydrophobic to Slippery

Abhijna Das, Kyoungjun Choi, Christelle Jablonski, Marcus Waser, Theodor Bühler, Junggou Kwon, Murray Height, and Renzo A. Raso**

A simple and efficient route to functionalize porous graphene is identified. The method enables the modification of porous graphene with varying surface properties ranging from lotus-like superhydrophobic surfaces to slippery surfaces. The method offers a route to superior membrane fabrication with versatile industrial applications. The findings clearly show the possibility of fabricating superhydrophobic surfaces with porous graphene as a base, which is relevant for oil-water separation and other membrane applications. The filament-like structures observed on the functionalized graphene mimic the properties of a lotus leaf. The measured water contact angle (WCA) of these modified surfaces reaches values as high as 160° with a contact angle hysteresis (CAH) below 10°, allowing for easy roll-off of water droplets. A Slippery behavior of the graphene surfaces is realized when the fibrillar structures on the graphene surfaces are infused with silicone oils. The work demonstrates the possibility of tuning the properties of graphene surfaces in a simple and efficient way and highlights possibly the first manufacturing method for graphene-based Slippery Liquid Infused Porous Surfaces (SLIPS).

1. Introduction

Often termed the "ultimate" membrane,[1] porous or perforated graphene can be a game-changer for various applications ranging from gas separation to water-proof membrane to oil-water separation.[1–3] The application of these graphene membranes depends primarily on their pore size distribution,[1–3] control over this parameter and the absence of any defects during their production is considered critical to preserve their exceptional membrane performance.[4] However, the production of these materials is not without its challenges as they are often synthesized via chemical vapor deposition (CVD) on metal catalysts and their subsequent assembly requires the transfer from the metallic surface onto a carrier material.[1–3] During their processing, defects can appear, which can be detrimental to the desired membrane properties.[5,6] To mitigate these issues and to improve their performance, many efforts have been dedicated to modifying the surface.[7,8] In this work, we specifically aimed to reinforce the graphene layer by growing silicone-based structures on the surface and simultaneously to modify its wettability. While there has been a lot of contention over the surface properties of graphene,[9,10] it is generally considered slightly hydrophobic due to the presence of airborne organic contaminants on the surface,[11] while clean free-standing graphene is reported to be hydrophilic.[12] Hence, targeted modifications of their hydrophobic properties can improve their performance specially for water-proof membrane applications and oil water separation.[13,14]

Here, we have used silanes to alter the surface properties of graphene surfaces. Silane chemistry is not new,[15,16] indeed for over a hundred years, silanes have been utilized to modify the properties of various surfaces,[17] including passivation/deactivation for chemical stability,[18] hydrophobization,[17,19] anti-fouling, and friction reduction.[18,20] Silanes have low surface energy, ideal for rendering a surface hydrophobic or even superhydrophobic. However, after the advent of per- and poly-fluoroalkyl substances (PFAS) in the 1940s,[21,22] silane chemistries were widely overlooked until recently, with a resurgence of silane chemistry as a viable alternative to harmful PFAS.[23] With that context, we have chosen the simplest form of silane chemistry to modify graphene surfaces. In the early 2000s, both Gao/McCarthy[24] and Artus/Seeger[25] introduced a hydrolyzation condensation reaction of chlorosilanes (especially trichloro silane) either by vapor phase[25] or in liquid phase[24] to introduce filamentary networks of silicones on surfaces.[24,25] Intriguingly, water drops deposited on these surfaces showed a contact angle of almost 180° leading to a virtually perfect spherical shape.[24] Since then, many studies have focused on these filamentary structures,[26] optimizing by changing process parameters such as solvents,[27] relative humidity,[26] time of

A. Das, K. Choi, C. Jablonski, M. Waser, T. Bühler, J. Kwon, R. A. Raso
Institute of Chemistry and Bioanalytics
University of Applied Sciences and Arts Northwestern Switzerland
Hofackerstrasse 30, Muttenz 4132, Switzerland
E-mail: abhijna.das@fhnw.ch; renzo.raso@fhnw.ch
M. Height
HeiQ Materials AG
Rütistrasse 12, Zurich 8952, Switzerland

The ORCID identification number(s) for the author(s) of this article can be found under https://doi.org/10.1002/admi.202400957

DOI: 10.1002/admi.202400957

reaction,[26] type of silanes[28–30] and have deposited them on a wide range of surfaces like polymers,[24,25,31] metals, and rough/woven surfaces such as textiles.[32–34]

Interestingly, these filamentary silicone structures were also deposited on reduced graphene oxide (rGO) coated cotton textiles in order to fabricate superhydrophobic textiles.[34] Similarly, in recent years, considerable efforts have been aimed toward the surface modification of graphene oxide (GO) and reduced graphene oxide (rGO) layers[35,36] to improve properties such as corrosion resistance,[37,38] improved bio compatibility,[39] and hydrophobicity.[34,38] One interesting study reported significant changes in the wettability of CVD graphene by introducing a high degree of wrinkles in the film through compression.[40] Another similar work extended on this approach by attaching octadecyl amine (ODA) to highly wrinkled few-layer graphene layers prepared on both flat and patterned silicon surfaces via microwave plasma CVD (MPCVD) after oxidizing it chemically.[41] With this method the wettability was varied by a wide range from hydrophilic to hydrophobic.[41] However, a significant gap still exists in transferring these processes to the field of chemical vapor-deposited graphene, partly due to an intrinsically inert chemical nature; hence they require some form of chemical,[41] plasma,[42] and doping[43] treatment prior to the chemical modification to make them receptive by introducing reactive groups in the basal plane, which in turn disrupts the sp^2 conjugation of the basal plane, essentially degrading the properties of the layer that make them so unique and robust.[44] Except for one contradictory report,[45] it is well-known that forming a siloxane network/brushes/monolayer on any surface depends on the presence of reactive groups such as hydroxyls to initiate/accelerate the reaction.[24,25] In that context, while pristine graphene without any structural defects[46] should not have any reactive group on the surface, porous graphene, on the other hand, can have multiple reactive groups, including —H, —OH, and —COOH,[47] due to the presence of edge type defects.[48] Hence, by exploiting these functional groups associated with the pores, we have introduced/accelerated silicone-based structures on the surface of porous graphene upon silanization. In this study, we show that the wetting properties of CVD-synthesized porous graphene can be controlled within minutes by a simple silanization process. Furthermore, by elucidating the kinetics of the silanization reaction, we can also predict the minimum reaction time required to obtain a superhydrophobic CVD synthesized porous graphene.[48] The role of edge defects in the kinetics of the reaction is also highlighted in this work. When the silanization reaction was carried out on a pristine graphene, drastic differences in the kinetics of the reaction and, consequently, their phenomenological behavior highlighted the role of functional groups in the growth kinetics of the filamentary structures. Additionally, further tweaking of the surface properties could be achieved by post-salinization infusion of oils, which led to the formation of a slippery-like layer.

2. Results and Discussion

Three different types of silanes, namely trichloromethyl silane (Tri-silane), dichlorodimethyl silane (Di-silane), and monochloro trimethyl silane (Mono-silane) were reacted on porous graphene surfaces. These silanes have three, two, or one hydrolysable chlorine atoms respectively. The hydrolysis of the Cl-group into a hydroxyl is responsible for the growth of different silane structures. Upon hydrolysis, condensation polymerization of the hydroxy silanes and elimination of water leads to continuous growth of siloxane structures. Previous studies have shown that depending on the silane type, either monolayer, brush layer, or network-type layer can be grown.[49] In this framework, we deposited three types of silanes during 1 h on as-grown porous graphene surface still attached onto the catalyst and porous graphene after transfer on a flat silicon substrate. The deposition procedure and removal of excess silanes after the deposition are explained in detail in the materials and methods section.

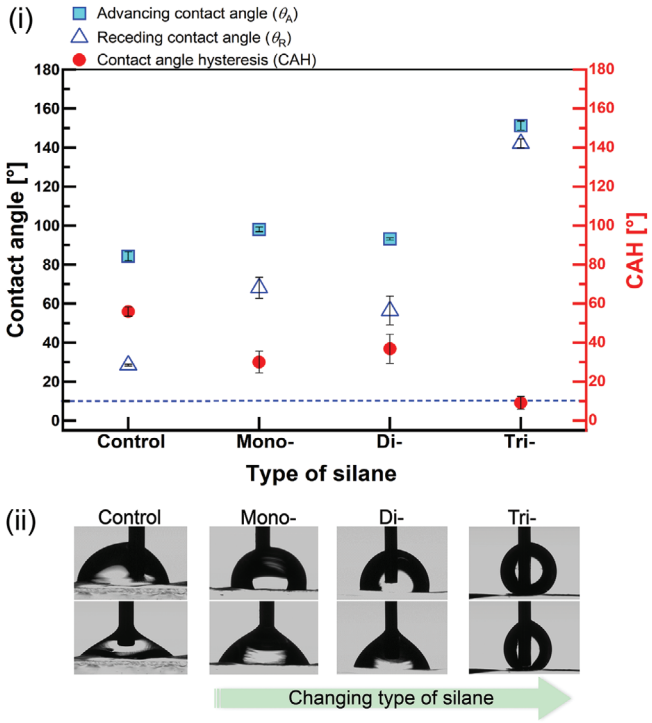

Figure 1. Influence of siloxane deposition on the wettability of the porous graphene surface. i) Contact angle of water measured on untreated and treated porous graphene (on copper substrate) plotted as a function of type of treatment (mono/di-silane/tri-silane). ii) Snapshots of the measurements visually representing the different behavior of water (advancing (top row) and receding (bottom row) contact angle) upon treatment: untreated sample (control), Monosilane-, Di-silane-, and Tri-silane-treated.

Next, we wanted to identify the influence of silane layer morphology and conformation upon phenomenological behavior, namely surface wettability. The dynamic contact angle of water was measured after the deposition and compared with the untreated surface. **Figure 1** shows the influence of siloxane condensation and deposition on the dynamic contact angle of water. Consistent with prior works,[9] non-porous graphene on a copper substrate shows an advancing contact angle of 84.2 ± 2.3° with very high contact angle hysteresis 28.4 ± 0.4°. The advancing contact angle is somewhat similar to the static contact angle and contact angle hysteresis indicates the ability of a drop to roll off – a qualitative indicator of the kinetic barrier associated with the removal of the contact line from a surface.[15] Literature instructs that to term a surface as superhydrophobic,[50,51] it has to

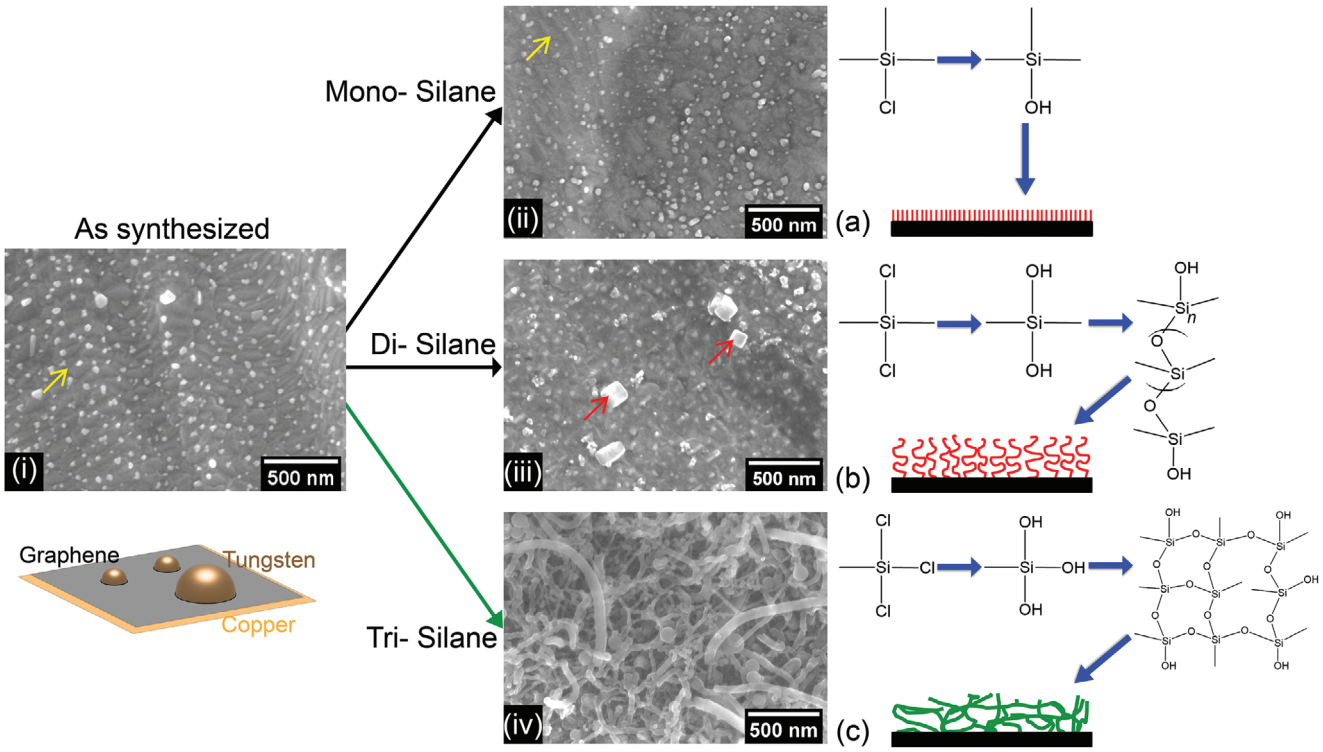

Figure 2. Influence of silane deposition on the morphological features of the modified graphene surface. SEM images of i) as synthesized single layer porous graphene (SLPG)/copper surface; SLPG/copper surface treated with ii) Monosilane, iii) Di-silane, and iv) Tri-silane respectively. Differences between the reactive groups and the mechanism of formation of different morphological features ranging from a) monolayer to b) a brush-like film (high surface density coverage), and to c) a network-like layer which possibly mimic the effects of a lotus leaf. The yellow arrows indicate the presence of wrinkling on the as synthesized graphene and the red arrows indicate the presence of cubic crystalline structures on the di-silane-treated porous graphene surface.

have a water contact angle of >150° with a contact angle hysteresis (CAH) of <10°, while slippery surfaces should show low CAH (<10°) to even low surface tension liquids.[51] Hence, we focused on measuring both contact angle and contact angle hysteresis. In this case, we measured the dynamic contact angle of water after the deposition of different silanes.

Di-type silane and mono-type silane did not demonstrate significant changes in the advancing contact angle. However, we could identify an increased receding contact angle, indicating the possibility of a type layer on the surface of graphene. Interestingly, a significant increase in the dynamic contact angle of water was observed with the introduction of tri-silane on the graphene layer. Starting from 84.2 ±2.3°, the advancing water contact angle increased to 151.2 ±2.4° with the introduction of tri-silane. More significantly, the CAH of water was as low as 9°, indicating the possibility of easy droplet roll-off. Such a high water contact angle is consistent with a roughness-induced contact angle originating from the Cassie-Baxter wetting state. Young´s contact angle of water on a surface of PDMS[52] is usually reported to be 105° – 110°. Logically, the following question arises: what is the cause of the contact angle behavior with different silane types? Perhaps more significantly, can we correlate their wettability to structural and morphological changes on the graphene surface coupled with the respective siloxane deposition?

To understand the origin of the significantly high contact angle associated with the tri-silane deposition process, we analysed the surface of the porous graphene with varying silane deposition and compared it with the porous graphene on copper (untreated control). Scanning electron microscopy (SEM) was used to investigate the changes in the morphological features of the graphene surface with the deposition of three types of silanes (deposition time = 1 h) to establish a correlation with their phenomenological behavior (**Figure 2**). The SEM images of the graphene on the metal catalyst showed the presence of tungsten nanoparticles (needed for the pore formation) and a wrinkled graphene layer (indicated by yellow arrows in Figure 2i). The wrinkling phenomenon of graphene on copper surfaces during its synthesis is often observed due to its higher thermal expansion coefficient relative to copper. Monosilane has only one reactive/hydrolysable group. Hence, when the chlorine atom hydrolyses in presence of water, it can only form monolayer domains surrounding the defect sites/pore edges, as condensation polymerization in this case cannot occur due to the structural constraint (Figure 2a). Consistently SEM images of the graphene layer obtained after the deposition of monosilane still show the presence of both the tungsten nanoparticles and the wrinkled regions of the graphene (yellow arrow in Figure 2ii), hinting toward a thin siloxane layer on the surface. SEM images of the di-silane deposited sample show the tungsten particles. However, the wrinkling features of the graphene film diminished noticeably after the condensation of the di-silane on the surface, indicating the presence of a thicker layer consistent with a brush

layer growth. It is to be noted that due to the presence of two chlorine atoms, the condensation polymerization after the hydrolysis can occur only in one direction (growth due to constraint) resulting in a brush layer growth (Figure 2b). Additionally, we could identify cubic crystal-like structures (highlighted in Figure 2iii by red arrows) on the surface that could be correlated with the unexpectedly lower receding contact angle with the di-silane deposition, as these areas allow for significant contact line pinning, increasing the contact angle hysteresis of water considerably.

Intriguingly, the tri-silane deposited graphene surface showed the presence of filamentary structures. Previous studies have also demonstrated that tri-silane tends to form filamentary structures due to a combination of the fast growth process and its reactivity.[24] Compared to their di- or mono- counterparts, the presence of three hydrolysable chlorine atoms in tri-silane makes them highly reactive (schematic Figure 2c). Hence, from a point of view of structure formation, the growth in this case occurs rapidly and in a random manner due to considerably higher degree of freedom of polymerization during the condensation process, which facilitates the formation of fibrillar structures. Through SEM analysis, we can observe a porous siloxane layer aided by the networks of filaments. The porosity of the surface originating from the tortuous arrangement of siloxane filaments promotes the formation of air pockets upon liquid droplet deposition, hence enabling the Cassie-Baxter wetting state. We also did not observe any changes in the contact angle value during the measurements, highlighting the absence of any transition from the Cassie-Baxter wetting state to the Wenzel wetting state, indicating a long-living metastable Cassie-Baxter wetting state. Furthermore, these filamentary siloxane structures covered the whole surface plane, demonstrating the homogeneity of the layer formation on graphene. Based on the findings of the three silane types, we focused on determining the kinetics of the deposition of the tri-type silane due to its exceptional superhydrophobic behavior.

Focusing on the deposition of these filamentary structures, we first wanted to identify the influence of the growth time on the homogeneity of the filamentary structures observed on the graphene film. Therefore, we varied the deposition time systematically from 0 to 1 h. We deposited the silanes before (Figure S1, Supporting Information) and after (**Figure 3**) the transfer of the porous graphene from the copper catalyst on silicon oxide (300 nm) substrates (without any surface treatment) to exclude the possible influence of copper/copper oxide from the growth mechanism of the filamentary structures. As expected, we measured a very low water contact angle and very high CAH when no silane was deposited. Already after 3 min reaction time, we observed a noticeable increase in the water contact angle. However, the CAH was still very high, but was eventually reduced to <5° after extension of the reaction time to 15 min. Interestingly, when plotting CAH as a function of reaction time (Figure 3i; Figure S1(i), Supporting Information), an exponential decay was observed. The following relation (Equation (1)) could be used to identify the influence of silane deposition time on their phenomenological behavior (CAH):

$$CAH_t = CAH_f + CAH_0\left(e^{-0.2t}\right) \quad (1)$$

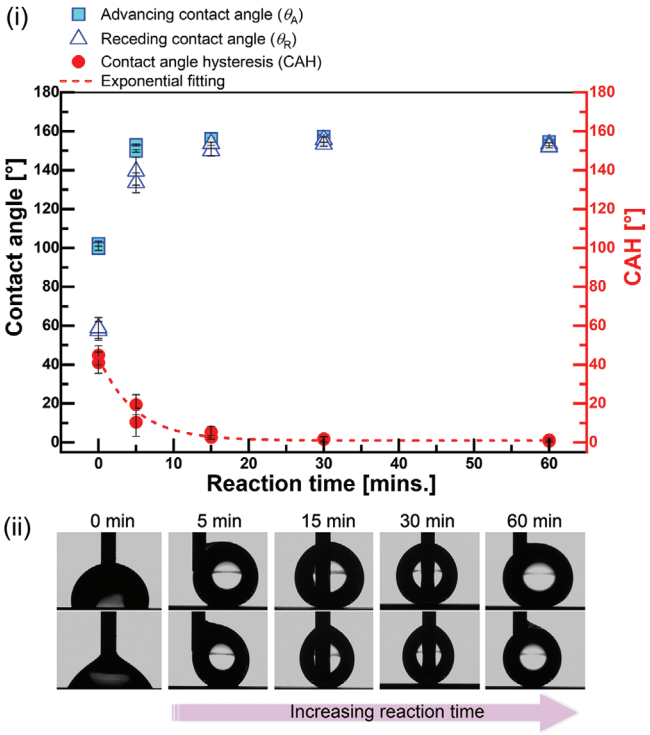

Figure 3. Influence of tri-silane reaction time on their phenomenological behavior. The experiments were carried out after transferring the porous graphene layer from metal catalyst onto silicon oxide substrates. i) Advancing (square) and receding (triangle) contact angle of water plotted as a function of silane deposition time (minutes). The CAH (circle) is plotted in the right y-axis as a function of deposition time. ii) Snapshot images of the contact angle measurements advancing (top row) receding (bottom row) with varying tri-silane reaction time (0 to 60 min).

where CAH_t (°) indicates the CAH measured at time t (minutes), CAH_0 is the CAH measured at time 0 (untreated surface), and CAH_f is the CAH measured at the final time point of the reaction (in this case 60 min). The equation was used to fit the CAH plot we obtained during our measurements, where we could identify that CAH decreased exponentially with an exponent of ca. -0.2 (min^{-1}). CAH is a phenomenological implication of the changes in the morphological and chemical features of the porous graphene surfaces. Hence, to understand this behavior, we need to elucidate the influence of the structural changes in the graphene film with the reaction time of tri-silane. So far, we have already established that the exceptionally low CAH and WCA can be associated with the presence of filamentary structures on the graphene film. Consequently, we investigated the influence of reaction time on the filamentary structures via scanning electron microscopy.

We first investigated the changes in the morphological features of the graphene surface with varying times of silane reaction on both graphene on copper catalyst and graphene after transfer on SiO_2 substrate (shown in **Figure 4**). SEM images of the samples were collected and analyzed with ImageJ to quantify the surface density coverage by the filamentary structures with varying deposition times. The SEM images revealed increased surface density of the filamentary structures with increased

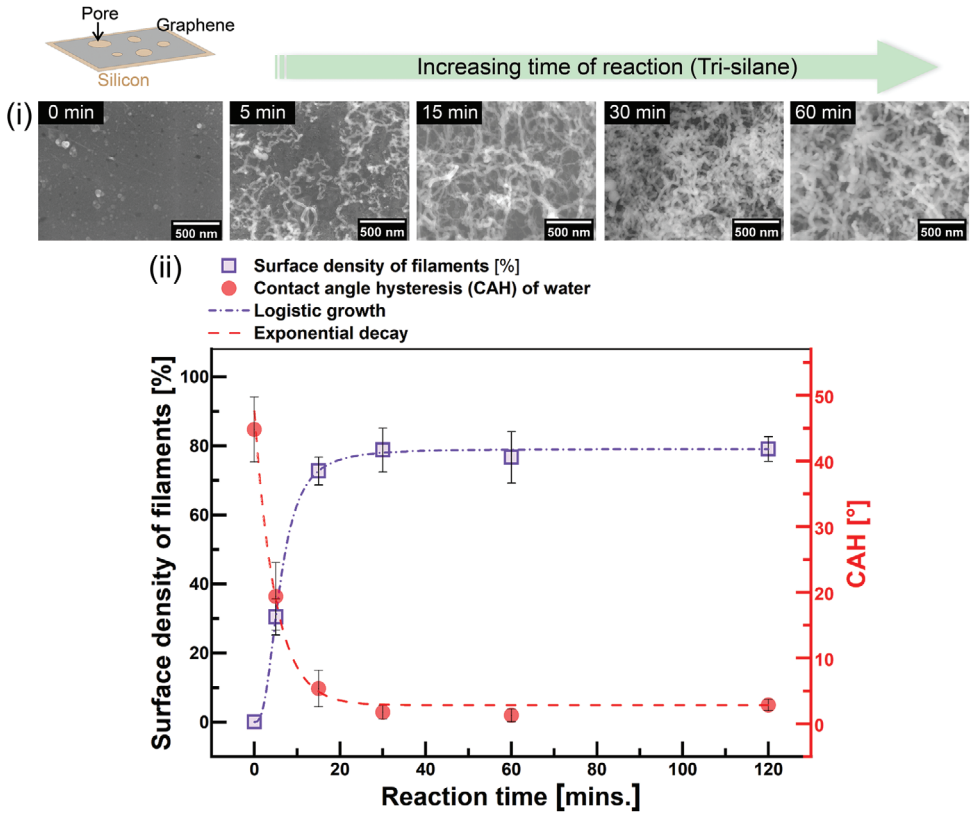

Figure 4. Influence of tri-silane deposition time on the surface coverage of the filamentary structures. i) The SEM images of the transferred graphene surface after 0, 5, 15, 30, and 60 min of tri-silane reaction. From the SEM images we can clearly identify changes in the surface coverage of the filamentary structures with varying reaction time. ii) Surface density of the filamentary structures on the surface plotted as a function of deposition time. The CAH measurements are plotted at the right y-axis, which shows a clear correlation between CAH measurements and the measured CAH of water.

reaction time. Very few filamentary structures were observed for 3 to 5 min reaction time in both cases (surface coverage ca. 30.5 ±5.3%). After plotting the surface covered by structures as a function of time, we could accurately correlate the percentage of coverage with the measured CAH data. As the area covered by the filamentary structure increased, the CAH decreased. While the surface coverage of the filamentary structures followed a logistic increase, the CAH followed an exponential decay with varying reaction times (Figure 4). We could achieve WCA as high as 157.3 ±0.4° and CAH as low as 1.5 ±1.4° with 78.8 ±6.4% surface coverage of these filamentary structures within 30 min of reaction. As discussed earlier, the CAH determines the ability of the drop to roll off a surface; for example, low CAH of water on a lotus leaf makes them superhydrophobic and self-cleaning.[53] The origin of low CAH of superhydrophobic surfaces is often attributed to hierarchical structures (roughness at different length scales);[54] here, the filamentary structure of the partially networked methyl siloxane provides the hierarchy necessary for easy roll-off. Hence, with increasing filamentary structures, we can observe decreasing CAH on CVD graphene surfaces allowing for precise tailoring of their wetting properties within 30 min of treatment.

It is worth noting that when we carried out the identical reaction of tri-silane on transferred pristine graphene surfaces (graphene without any pores), the superhydrophobic effect was not so evident, notably since the CAH remained very high even with 1 h of deposition time (see Figures S2 and S3, Supporting Information). Further analysis with SEM revealed the presence of uneven surface coverage of the filamentary structures even after 1 h of deposition. Such an observation suggests that the edge defects on the porous surface may accelerate the formation of the filamentary structures during the reaction of tri-silane.

While we could observe the logistic growth of the filamentary structures with increasing deposition time, there is still a probability of growth of the filamentary structures in the z-direction. Hence, it is important to investigate the growth perpendicular to the basal plane surface. Confocal laser scanning microscopy (CLSM) was used to characterize the roughness changes associated with tri-silane deposition. In fact, previous work on CLSM on CVD graphene surfaces demonstrated its efficiency in measuring parameters such as thickness variation, wrinkling, and roughness.[55] Roughness was calculated by using both, line roughness (line length = 32 µm, minimum 20 measurements) and area roughness (25 × 25 µm^2, minimum 3 measurements) data. Line roughness data is presented here, while the area roughness along with the images of the samples are shown in the supporting information. The average roughness (R_a) and the rms roughness (R_q) of untreated surfaces were ca. 2.5 nm and ca. 3.1 nm, respectively, consistent with single layer or few layers porous graphene surfaces. Significant increase in the roughness values was observed with varying silane reaction times. Higher roughness indicates growth in the z-direction due to the presence of fibers, further increase in the roughness values observed with

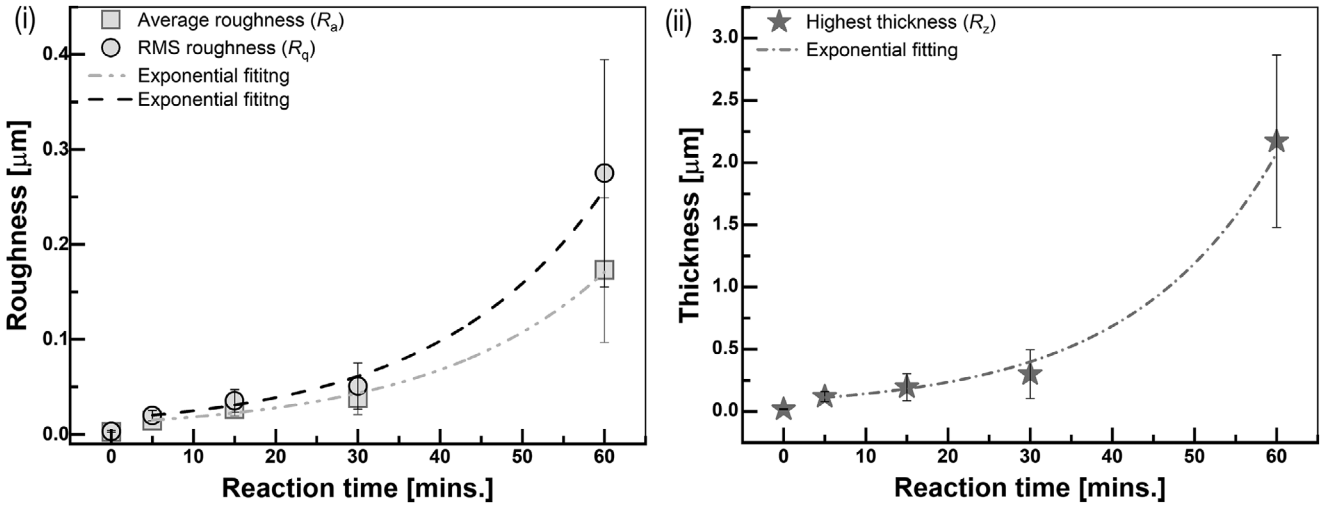

Figure 5. i) Average roughness (R_a, square) and the RMS roughness (R_q, circle) of the layer of silica filament like structures grown on SLPG graphene as a function of reaction time. ii) Roughness parameter (R_Z, star) plotted as a function of reaction time.

increasing reaction times might explain the logistic growth observed in this study. When we plotted both R_q and R_a as a function of reaction time (**Figure 5**(i)), we could observe an exponential growth with time (Figure 5(i)). Additionally, we also calculated the maximum height of the layers (R_z) which also showed exponential growth over time (Figure 5(ii)), implying that while the surface coverage in the x-y plane reached a plateau within 15 min, the filamentary structures continued to grow perpendicularly in the z-axis (as evident by the exponential increase of roughness with time), pointing to the potential of continuous growth of the silane filament carpet.

Additionally, we measured the FTIR spectra (at a grazing angle of 83°) of the graphene surfaces with varying deposition times (**Figure 6**(i)) using Agilent Spectrometer Cary 680 and Agilent Microscope 620 with a grazing angle objective (128 scans and a spectral resolution of 4 cm^{-1}). We used the samples transferred onto a silicon oxide substrate for roughness measurements and the FTIR analysis to assess the content of hydrophobic species. From the FTIR spectra (base line corrected using Resolution Pro V.5.4.1 software), we could identify two peaks associated with the growth of the filamentary structures: one associated with the stretching vibration of the CH bonds at 2962 cm^{-1} related to the methyl groups[56] and the other associated with the symmetric deformation of CH_3 in the Si-CH_3 groups[56] at 1259 cm^{-1}. The Si-CH_3 groups are associated to the partially networked methyl siloxane chains formed during the polymerization condensation process of the tri-silane. The notable absence of these two peaks in the spectra of the untreated porous graphene surface confirmed

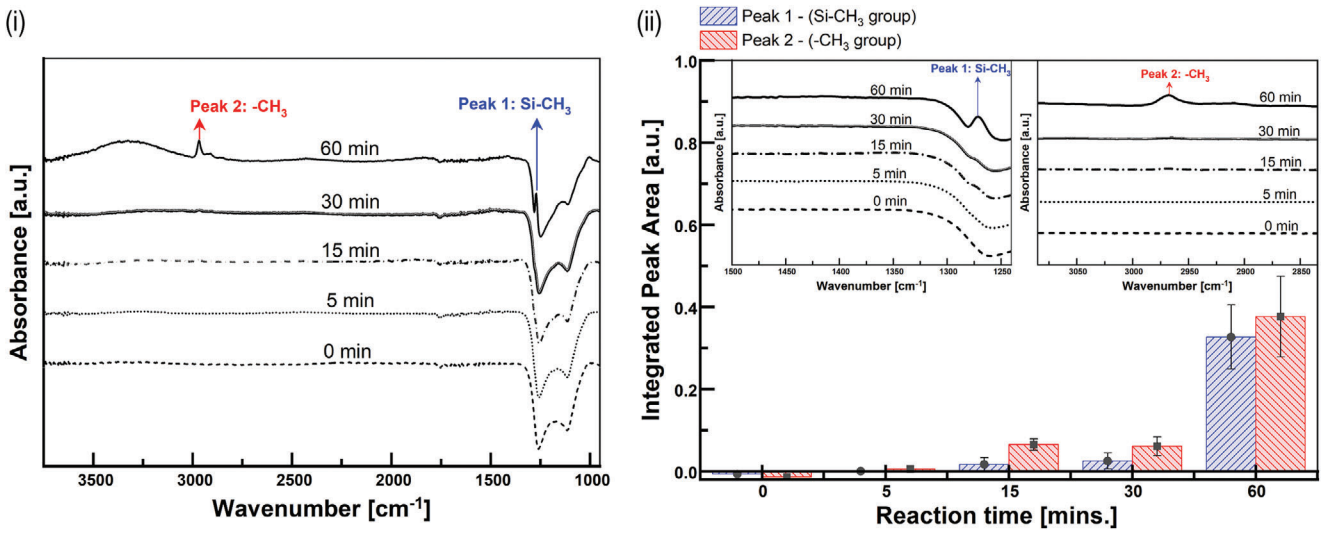

Figure 6. i) FTIR spectra of the graphene surface modified with tri-silane for different times. The peak observed at wavenumber 2962 cm^{-1} indicate the presence of —CH_3 groups and peak observed at wavenumber 1259 cm^{-1} originate from the symmetric deformation of methyl groups in Si-CH_3 indicating the presence of silanes on the graphene surface. ii) Integrated peak areas of peak 1 and 2 of the FTIR spectra (shown as inset) plotted with respect to reaction time (minutes) showing a systematic increase over time indicating increased formation of the filamentary structures.

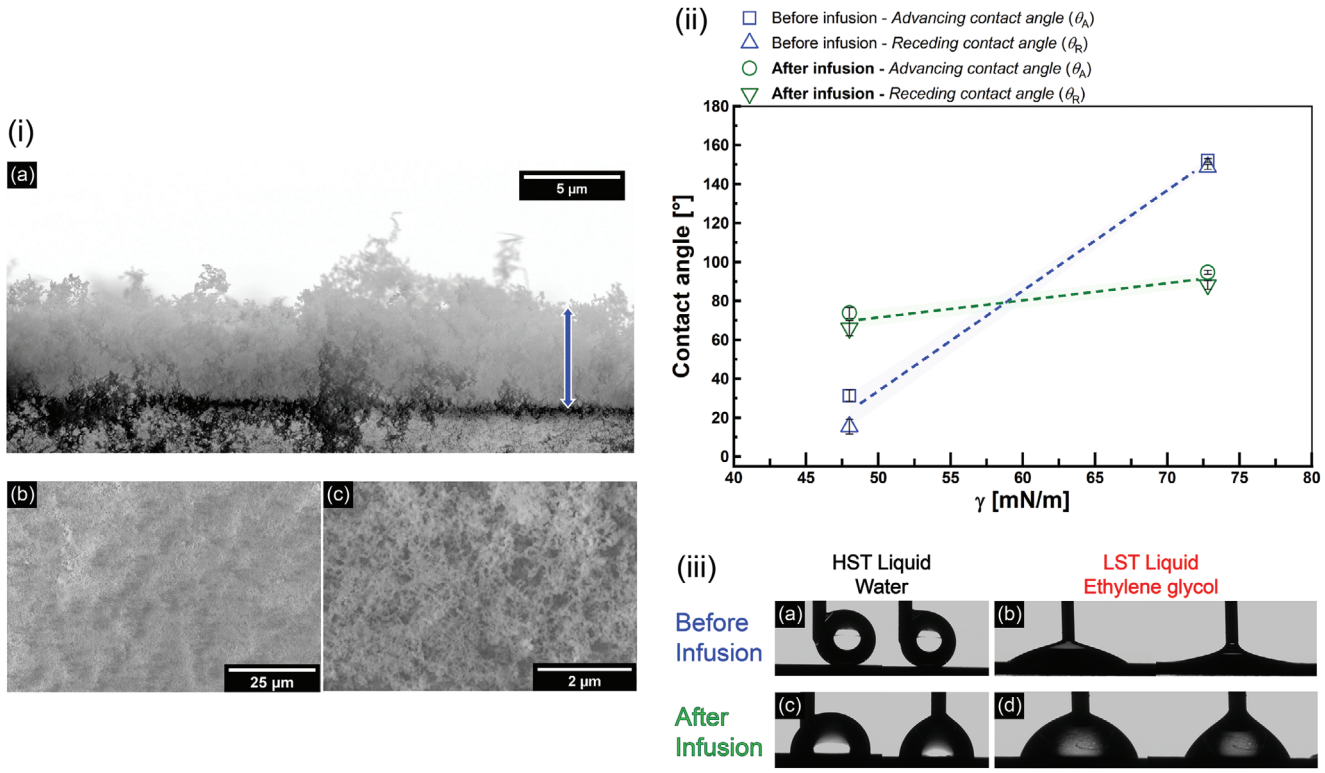

Figure 7. Observations of a slippery graphene-based layer. (i) (a) Cross-section and b,c) top view of the Tri-silane modified (reaction time ca. 240 min) graphene surface visualized through SEM. The scale bars are specified in each image. The cross-section image clearly shows that the thickness of the filamentary silane layer is ≥5 µm. (ii) The dynamic contact angle and contact angle hysteresis (CAH) of ethylene glycol (γ = 48 mN/m) and water (γ = 72.8 mN/m) on Tri-silane modified graphene before and after infusion of silicone oil. (iii) Snapshots of advancing (left) and receding (right) water (a,c) and ethylene glycol (b,d) droplets before (a,b) and after (c,d) the infusion of silicone oil.

conclusively that these two peaks indeed originate from the filamentary structures. As such they can be tracked to follow the siloxane grow reaction on the porous graphene surface.

The intensity of the two peaks is associated with the systematic increase in deposition time (shown in Figure 6(ii)). The area under the peak at 2962 and 1259 cm^{-1} was integrated using Resolution Pro V.5.4.1 software. We could observe a systematic increase in their area with the increase in the deposition time that is associated to the growing of filaments with increasing reaction time. The correlation between the roughness measurements and the FTIR spectra over time points explicitly to the z-axis growth of the filaments with increasing time of deposition. This follows from the increased pathlength of the IR beam through the filamentous structure in the grazing angle FTIR set up. Our observations suggest that not only the surface coverage but also the thickness of the filamentary layer can be controlled by the reaction time, which might be critical in the design of graphene-based waterproof membranes (specifically for properties such as hydrostatic pressure resistance).

While superhydrophobic properties on a graphene surface can open the pathway to myriads of functional membrane applications, we also aimed to explore the potential of making graphene-based surfaces repellent to low surface tension liquids. One of many explored omni-repellent surfaces, Slippery Liquid Infused Porous Surfaces (SLIPS) have been quite prominent due to their simple approach and elegant physics. SLIPS is a bioinspired surface mimicking the slippery nature of the Nepenthes Pitcher plant,[57] where the patterned leaves surfaces are usually infused with water, leading to insects slipping in the plant funnel after landing on the leaf. Based on their structure, the Aizenberg research group first demonstrated a porous surface's ability in repelling a comprehensive range of surface tension liquids when these surfaces were infused with either silicone or fluorinated oils.[58] Recently, these types of silane-based filamentary structures were also infused with silicone-based[59] or fluorine based oils[60,61] to demonstrate the slipperiness of the infused surfaces arising from a liquid/liquid interface.

Inspired by these studies, we wanted first to grow the filamentary structures as thick as possible to minimize the leaching of the oil from the structures; hence, the reaction time was increased to 4 h. After 4 h of reaction with tri-silane, we observed a carpet of these filamentary structures as thick as 5 µm in some regions (**Figure** 7i(a–c)). Next, we infused these structures with a silicone oil of relatively low viscosity (100 cSt), and we could observe effective spreading of the oil on the surface consistent with infusion into the filamentary structures. The samples were kept under vacuum and then rinsed with water to remove excess oil. We measured the dynamic contact angle of both water and ethylene glycol. We deliberately chose two liquids with very different surface tension, one representing the highest possible and the other representing the lower surface tension liquids. Before the infusion of oil, the advancing water contact angle was almost 152°, and the

CAH was 3°, demonstrating a lotus leaf-type effect. When we deposited a drop of ethylene glycol ($\gamma = 48$ mN/m), the drop spread quickly on the surface with an advancing contact angle of 31° and CAH of 15°. Such a high CAH indicates a spreading behavior of low surface tension liquids, possibly indicating a transition of Cassie-Baxter to Wenzel state. Consistent with previous studies that have observed the lotus-leaf effect, these surfaces are ineffective for low surface tension liquids due to a relatively unstable Cassie-Baxter state, leading to a transition to the Wenzel state as the liquid penetrates the porous structure.

Notably, we observed a very different wetting behavior of both water and ethylene glycol after the infusion of oil. The advancing contact angle of water decreased significantly due the infused silicone oil. Still, the CAH of water remained <10°, which is indicative of a slippery surface. Furthermore, we also did not observe any oil film residue on the water droplet (also known as "cloaking" phenomenon)[62] during the measurement. When ethylene glycol drops were dosed on the surface, we observed a noticeably higher advancing contact angle, indicating no penetration of the drop, and the CAH remained <10°. Lower CAH and high contact angle of ethylene glycol points to a liquid/liquid interface where the angle of ethylene glycol drop arises from the classical young's contact angle on a liquid/liquid interface. To the best of our knowledge, this work provides the first description for fabricating graphene-based SLIPS. Our findings demonstrate the possibility of modifying graphene surfaces focused on various coating applications specifically for water/oil repellence. While this is the first proof-of-concept demonstration of graphene-based SLIPS, future work is expected to expand this methodology to identify the influence of viscosity, the chemical structure of the lubricant (oil), and thickness of the silane network on their slippery behavior.

3. Conclusion

This study outlines a simple approach for modifying the wetting properties of graphene surfaces. By varying the silane type, we obtained three types of morphology on the graphene surface. During the deposition and condensation polymerization process of different types of silanes, monosilane formed an ultra-thin layer, di-silane formed a thicker layer on the surface, and trisilane formed a thick layer consisting of filamentary structures. The filamentary structures formed during the deposition of trisilane dramatically influenced the hydrophobicity of the surface. The low surface energy, along with the hierarchical roughness associated with the filamentary structures, led to a long-lasting metastable Cassie-Baxter wetting state, which increased the water contact angle.

Interestingly, depending on the presence or absence of pores on the graphene surface, the surface coverage of the filamentary structures differed significantly with identical deposition time of the tri-silane, highlighting the role of pore edges in promoting the growth. Aided by the abundance of functional groups present at the edges of the graphene pores,[46,63] within 15 min of deposition of tri-silane, we were able to increase the WCA on these porous graphene surfaces from 90° to almost 160°. When the tri-silane was reacted on porous graphene surfaces, we could observe an exponential decay of the CAH with deposition time, which corresponded with a logistic increase of the surface coverage of the filamentary structures, emphasizing the control over the surface properties of these graphene-siloxane hybrid surfaces. We could also identify the vertical growth dynamic of these filamentary structures, suggesting the possibility of thickness control of the "siloxane-filament carpet" on the porous graphene surfaces. A simple approach for fabricating graphene-based SLIPS was also demonstrated here, by simply infusing silicone oil into a very thick siloxane-filament carpet on the graphene surfaces. We could show that the CAH was <10° for both high (water) and low (ethylene glycol) surface tension liquids when the filamentary structures were infused with a silicone oil lubricant.

In this study, we have explored the efficacy of silanes on modifying porous and pristine graphene surfaces. The outlined approach is simple, easy to use, and readily scalable. This approach also allows for tweaking of surface properties of graphene ranging from superhydrophobic to slippery surface in a controllable manner, which offers potential use toward the fabrication of state-of-the-art graphene-based membranes for various applications.

4. Experimental Section

Synthesis of Porous Graphene: The synthesis of chemical vapor deposited (CVD) porous graphene is mentioned in detail elsewhere.[48] Essentially, this method follows a bottom-up approach where nanoparticles of tungsten (W) are formed on top of the copper (Cu) catalyst. Graphene was subsequently synthesized by CVD on the W free area of the catalyst surface leaving pores upon the removal of the W nanoparticles (droplets) at the end of the process. In brief, a W film of 2 nm was coated on bare Cu foil (Alfa Aesar 46986, 99.8% purity) using a plasma sputter coater (FHR Pentaco 100) at a pressure of 0.002 mbar, with 100 standard cubic centimeters per minute (sccm) of Ar under 0.25 kW of DC plasma. Before the coating process, the Cu foil (Alfa Aesar 46986, 99.8% purity) was treated with an Ar-ion beam for 10 min to reduce the surface roughness of the copper foil. The treated W/Cu catalyst was kept within a Cu envelope (Alfa Aesar 46986) for further processing. The W/Cu catalyst in the Cu envelope was placed at the center of a low-pressure chemical vapor deposition (CVD) furnace. The W/Cu in the Cu envelope was first annealed at 950 °C in the CVD chamber for 30 min under a flow of 50 sccm of H_2 that enabled spinodal dewetting of the W layer resulting in smaller droplets on the catalyst. Following annealing, graphene synthesis was initiated at the identical temperature by introducing a mixture of 4 sccm of CH_4 and 50 sccm of H_2 at 800 mTorr for 10 min. The sample was then gradually cooled to room temperature while maintaining a flow of 100 sccm of H_2. Nucleation and growth of graphene was inhibited in the areas where W droplets are present[48] resulting in the formation of pores when the graphene is transferred to a desired substrate.

Synthesis of Pristine Graphene: For the synthesis of non-porous/pristine graphene the copper catalyst was purchased from JX Metals. In this case, the Cu could be used as received (without pretreatment) for the synthesis process. A small part of the foil was cut and placed at the center of the CVD furnace. Here, the annealing of the Cu was done at 1000 °C for 20 min under a flow of 50 sccm of H_2. Subsequently, the graphene was synthesized at an identical temperature by introducing a mixture of 50 sccm of CH_4 and 10 sccm of H_2 flow for 45 min. After the growth was completed, the sample was gradually cooled down to room temperature with 20 and 100 sccm of H_2 and Ar flow, respectively.

Transfer of Graphene onto Silicon Substrates: Transfer of the graphene from the metal catalyst was achieved by etching off the catalyst substrate. This kind of transfer process of graphene requires a supporting layer to preserve the layer from disintegrating and minimize defects. During the transfer process, a thick layer of spin-coated poly(methylmethacrylate) (PMMA) was used as a supporting layer. The Cu catalyst and the W droplets were etched by floating the samples (with spin coated PMMA

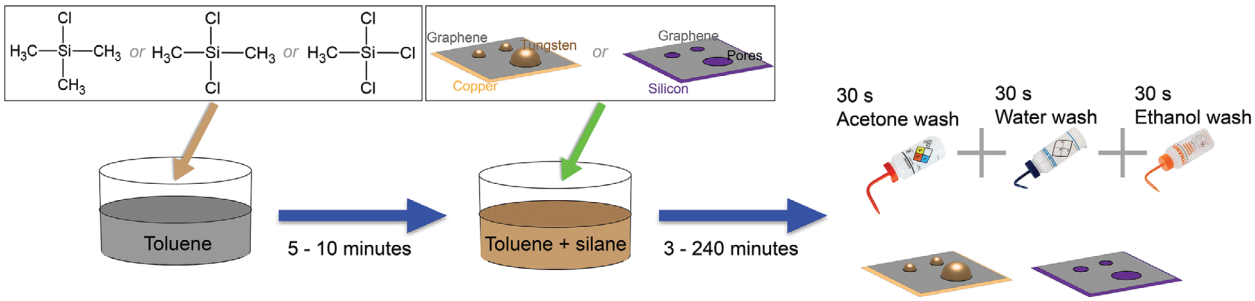

Figure 8. Schematic diagram of the silane reaction process.

layer) on an aqueous 0.5M ammonium persulfate $(NH_4)_2S_2O_8$ (APS, Sigma–Aldrich) bath with the Cu side at the interface. After 10 min, the samples were washed with water and wiped with lint-free tissue to remove the backside graphene formed during the CVD process. Afterward, the samples were placed back on the etching bath for 3 h. The sample was then floated on a water bath for 1 h to remove the APS residues when no copper residue was visible on the sample. The sample was then picked up using a silicon dioxide substrate. The removal angle was maintained at 45° to ensure conformal adhesion of the graphene with the substrate. After sufficient drying, the PMMA layer was dissolved by placing the sample in an acetone bath (Sigma–Aldrich) for 1 h, and then the sample was dried with nitrogen flow.

Growth of Siloxane Filaments: Silanized-Graphene samples were prepared by immersion in a silane/toluene solution. Monochloro trimethyl silane (Monosilane), Dichloro dimethyl silane (Di-silane), and Trichloro methyl silane (Tri-silane) and solvents such as toluene, acetone, and ethanol (all HPLC grade) were purchased from Sigma Aldrich. The concentration of silane in toluene was kept constant in all cases at 0.01 g ml^{-1}. Toluene was chosen as the desired solvent for the deposition process due to the low water solubility and content in order to prevent rapid hydrolysis of the chlorosilanes. The samples, i) graphene as prepared on copper catalyst and ii) graphene transferred to silicon substrate by etching process, were immersed in the 0.01 g ml^{-1} of chlorosilane/toluene solution for varying time periods ranging from 3 min to 4 h maximum. After immersion, the samples were rinsed immediately by a jet flow of acetone for 30 s, followed by a cleaning jet flow with water and subsequently ethanol for 30 s, respectively. The order of the rinsing process is kept constant throughout this study. The cleaning process removes both the excess and unreacted silanes from the surface. After the cleaning process the samples were dried under an argon/nitrogen flow at room temperature (30 s). The schematic diagram of the process is shown in **figure 8**.

Contact Angle Measurements: The dynamic contact angle measurements were carried out by increasing (advancing) and reducing (receding) the volume of a sessile drop (Krüss DSA 10 mK2 drop shape analyser system). After placing a sessile drop of 2 µl in volume on the sample's surface (using a 0.5 mm diameter syringe needle), 6 µl of the desired liquid was continuously dosed at a rate of 20 µl min^{-1}. A video was recorded of the drop during the dosing process (CCD camera, 12.5 fps, total number of frames = 180) to measure the advancing contact angle. After the dosing process, the liquid was retracted at an identical rate, and another video was recorded with identical parameters during the retraction process. Each frame of the video was analyzed using the drop shape analyzer software, and the tangent method was used to measure the contact angle of each frame. The contact angle values presented here were averaged from all the frames acquired during the measurement, where the error bars represent the variation of contact angles within the acquired frames (figure 8).

Supporting Information

Supporting Information is available from the Wiley Online Library or from the author.

Acknowledgements

The authors are grateful to Innosuisse Research Council for their generous financial support. The authors gratefully acknowledge the financial contribution from the Innosuisse through the project Swiss HIPOGRAPH (project number: 45921.1 IP-ENG).

Conflict of Interest

Two patents have been filed based on the findings of our research (EP24180719 and EP24209916). Dr. Murray Height is co-founder of HeiQ Materials AG.

Data Availability Statement

The data that support the findings of this study are available from the corresponding author upon reasonable request.

Keywords

graphene membrane, graphene SLIPS, porous graphene, silanization, superhydrophobic

Received: November 28, 2024
Revised: January 17, 2025
Published online: February 10, 2025

[1] K. Celebi, J. Buchheim, R. M. Wyss, A. Droudian, P. Gasser, I. Shorubalko, J.-I. Kye, C. Lee, H. G. Park, *Science* **2014**, *344*, 289.
[2] D. Jang, J.-C. Idrobo, T. Laoui, R. Karnik, *ACS Nano* **2017**, *11*, 10042.
[3] T. Ashirov, A. O. Yazaydin, A. Coskun, *Adv. Mater.* **2022**, *34*, 2106785.
[4] S. C. O'Hern, C. A. Stewart, M. S. H. Boutilier, J.-C. Idrobo, S. Bhaviripudi, S. K. Das, J. Kong, T. Laoui, M. Atieh, R. Karnik, *ACS Nano* **2012**, *6*, 10130.
[5] M. S. H. Boutilier, C. Sun, S. C. O'Hern, H. Au, N. G. Hadjiconstantinou, R. Karnik, *ACS Nano* **2014**, *8*, 841.
[6] S. Huang, M. Dakhchoune, W. Luo, E. Oveisi, G. He, M. Rezaei, J. Zhao, D. T. L. Alexander, A. Züttel, M. S. Strano, K. V. Agrawal, *Nat. Commun.* **2018**, *9*, 2632.
[7] A. Criado, M. Melchionna, S. Marchesan, M. Prato, *Angew. Chem., Int. Ed.* **2015**, *54*, 10734.
[8] C. Wetzl, A. Silvestri, M. Garrido, H.-L. Hou, A. Criado, M. Prato, *Angew. Chem., Int. Ed.* **2023**, *62*, 202212857.
[9] J. Rafiee, X. Mi, H. Gullapalli, A. V. Thomas, F. Yavari, Y. Shi, P. M. Ajayan, N. A. Koratkar, *Nat. Mater.* **2012**, *11*, 217.
[10] D. Parobek, H. Liu, *2D Mater.* **2015**, *2*, 32001.

[11] Z. Li, Y. Wang, A. Kozbial, G. Shenoy, F. Zhou, R. McGinley, P. Ireland, B. Morganstein, A. Kunkel, S. P. Surwade, L. Li, H. Liu, *Nat. Mater.* **2013**, *12*, 925.
[12] A. V. Prydatko, L. A. Belyaeva, L. Jiang, L. M. C. Lima, G. F. Schneider, *Nat. Commun.* **2018**, *9*, 4185.
[13] Z. Chu, Y. Feng, S. Seeger, *Angew. Chem., Int. Ed.* **2015**, *54*, 2328.
[14] H. M. Mousa, H. S. Fahmy, G. A. M. Ali, H. N. Abdelhamid, M. Ateia, *Adv. Mater. Interfaces* **2022**, *9*, 2200557.
[15] L. Gao, T. J. McCarthy, *Langmuir* **2006**, *22*, 5998.
[16] D. Pakuła, B. Marciniec, R. E. Przekop, *AppliedChem* **2023**, *3*, 89.
[17] L. Li, B. Li, J. Dong, J. Zhang, *J. Mater. Chem. A* **2016**, *4*, 13677.
[18] B. J. Melde, A. P. Malanoski, M. H. Moore, B. J. Johnson, *Polym. Int.* **2021**, *70*, 701.
[19] I. S. Bayer, *Adv. Mater. Interfaces* **2020**, *7*, 2000095.
[20] B. Khatir, Z. Azimi Dijvejin, P. Serles, T. Filleter, K. Golovin, *Small* **2023**, *19*, 2301142.
[21] J. Glüge, M. Scheringer, I. T. Cousins, J. C. DeWitt, G. Goldenman, D. Herzke, R. Lohmann, C. A. Ng, X. Trier, Z. Wang, *Environ. Sci. Process. Impacts* **2020**, *22*, 2345.
[22] L. G. T. Gaines, *Am. J. Ind. Med.* **2023**, *66*, 353.
[23] I. T. Cousins, G. Goldenman, D. Herzke, R. Lohmann, M. Miller, C. A. Ng, S. Patton, M. Scheringer, X. Trier, L. Vierke, Z. Wang, J. C. DeWitt, *Environ. Sci. Process. Impacts* **2019**, *21*, 1803.
[24] L. Gao, T. J. McCarthy, *J. Am. Chem. Soc.* **2006**, *128*, 9052.
[25] G. R. J. Artus, S. Jung, J. Zimmermann, H.-P. Gautschi, K. Marquardt, S. Seeger, *Adv. Mater.* **2006**, *18*, 2758.
[26] G. R. J. Artus, S. Seeger, *Adv. Colloid Interface Sci.* **2014**, *209*, 144.
[27] J. Zhang, L. Li, B. Li, S. Seeger, *RSC Adv.* **2014**, *4*, 33424.
[28] Gao, T. J. McCarthy, *Langmuir* **2008**, *24*, 362.
[29] J. Zhang, A. Wang, S. Seeger, *Polym. Chem.* **2014**, *5*, 1132.
[30] J. Zimmermann, M. Rabe, G. R. J. Artus, S. Seeger, *Soft Matter* **2008**, *4*, 450.
[31] Z. Liu, X. Pang, K. Wang, X. Lv, X. Cui, *ACS Appl. Mater. Interfaces* **2019**, *11*, 22809.
[32] J. Zimmermann, F. A. Reifler, G. Fortunato, L.-C. Gerhardt, S. Seeger, *Adv. Funct. Mater.* **2008**, *18*, 3662.
[33] J. Zhang, S. Seeger, *Adv. Funct. Mater.* **2011**, *21*, 4699.
[34] M. Shateri-Khalilabad, M. E. Yazdanshenas, *Cellulose* **2013**, *20*, 963.
[35] J. H. Lee, S. H. Kim, *Sci. Rep.* **2020**, *10*, 19152.
[36] S. S. Ashok Kumar, S. Bashir, K. Ramesh, S. Ramesh, *FlatChem* **2022**, *31*, 100326.
[37] A. Ahmadi, B. Ramezanzadeh, M. Mahdavian, *RSC Adv.* **2016**, *6*, 54102.
[38] M. J. Nine, M. A. Cole, L. Johnson, D. N. H. Tran, D. Losic, *ACS Appl. Mater. Interfaces* **2015**, *7*, 28482.
[39] S. S. R. Vuppaladadium, T. Agarwal, S. Kulanthaivel, B. Mohanty, C. S. Barik, T. K. Maiti, S. Pal, K. Pal, I. Banerjee, *Mater. Sci. Eng. C* **2020**, *110*, 110647.
[40] J. Zang, S. Ryu, N. Pugno, Q. Wang, Q. Tu, M. J. Buehler, X. Zhao, *Nat. Mater.* **2013**, *12*, 321.
[41] J. Dong, Z. Yao, T. Yang, L. Jiang, C. Shen, *Sci. Rep.* **2013**, *3*, 1733.
[42] A. Jafari, H. R. Mortaheb, F. Gallucci, *Chem. Eng. Res. Des.* **2022**, *187*, 251.
[43] H. Liu, Y. Liu, D. Zhu, *J. Mater. Chem.* **2011**, *21*, 3335.
[44] H. Terrones, R. Lv, M. Terrones, M. S. Dresselhaus, *Reports Prog. Phys.* **2012**, *75*, 062501.
[45] E. Kasapgil, E. G. Atici, R. Cicek, I. Anac, H. Y. Erbil, *RSC Adv.* **2016**, *6*, 74921.
[46] F. Banhart, J. Kotakoski, A. V. Krasheninnikov, *ACS Nano* **2011**, *5*, 26.
[47] D. W. Boukhvalov, M. I. Katsnelson, *Nano Lett.* **2008**, *8*, 4373.
[48] K. Choi, A. Droudian, R. M. Wyss, K.-P. Schlichting, H. G. Park, *Sci. Adv.* **2018**, *4*, eaau0476.
[49] A. K. Halvey, B. Macdonald, K. Golovin, M. Boban, A. Dhyani, D. H. Lee, J. W. Gose, S. L. Ceccio, A. Tuteja, *ACS Appl. Mater. Interfaces* **2021**, *13*, 53171.
[50] J. Bico, C. Marzolin, D. Quéré, *Europhys. Lett.* **1999**, *47*, 220.
[51] H.-J. Butt, J. Liu, K. Koynov, B. Straub, C. Hinduja, I. Roismann, R. Berger, X. Li, D. Vollmer, W. Steffen, M. Kappl, *Curr. Opin. Colloid Interface Sci.* **2022**, *59*, 101574.
[52] B. Ruben, M. Elisa, L. Leandro, M. Victor, G. Gloria, S. Marina, S. Mian K, R. Pandiyan, L. Nadhira, *Micro Nano Lett* **2017**, *12*, 754.
[53] W. Barthlott, C. Neinhuis, *Planta* **1997**, *202*, 1.
[54] B. Bhushan, Y. C. Jung, *Prog. Mater. Sci.* **2011**, *56*, 1.
[55] V. Panchal, Y. Yang, G. Cheng, J. Hu, M. Kruskopf, C.-I. Liu, A. F. Rigosi, C. Melios, A. R. Hight Walker, D. B. Newell, O. Kazakova, R. E. Elmquist, *Commun. Phys.* **2018**, *1*, 83.
[56] J. Lee, J. Kim, H. Kim, Y. M. Bae, K.-H. Lee, H. J. Cho, *J. Micromechanics Microengineering* **2013**, *23*, 035007.
[57] H. F. Bohn, W. Federle, *Proc. Natl. Acad. Sci. USA* **2004**, *101*, 14138.
[58] T.-S. Wong, S. H. Kang, S. K. Y. Tang, E. J. Smythe, B. D. Hatton, A. Grinthal, J. Aizenberg, *Nature* **2011**, *477*, 443.
[59] E. Kasapgil, I. Anac, H. Y. Erbil, *Colloids Surfaces A Physicochem. Eng. Asp.* **2019**, *560*, 223.
[60] J. Zhang, L. Wu, B. Li, L. Li, S. Seeger, A. Wang, *Langmuir* **2014**, *30*, 14292.
[61] J. Zhang, A. Wang, S. Seeger, *Adv. Funct. Mater.* **2014**, *24*, 1074.
[62] A. A. Günay, S. Sett, Q. Ge, T. Zhang, N. Miljkovic, *Adv. Mater. Interfaces* **2020**, *7*, 2000983.
[63] M. D. Bhatt, H. Kim, G. Kim, *RSC Adv.* **2022**, *12*, 21520.